Observation of strong correlation between quasimonoenergetic electron beam generation by laser wakefield and laser guiding inside a preplasma cavity

Tomonao Hosokai,* Kenichi Kinoshita, Takeru Ohkubo, Akira Maekawa, and Mitsuru Uesaka
Nuclear Professional School, Graduate School of Engineering, University of Tokyo, 22-2 Shirane-shirakata, Tokai, Naka, Ibaraki 319-1188, Japan

Alexei Zhidkov†
Department of Accelerator Physics and Engineering, National Institute of Radiological Sciences, 4-9-1, Anagawa, Inage, Chiba 263-8555, Japan

Atsushi Yamazaki
Institute for Chemical Research, Kyoto University, Gokasho, Uji, Kyoto 611-0011, Japan

Hideyuki Kotaki, Masaki Kando, Kazuhisa Nakajima, and Sergei V. Bulanov†
Advanced Photon Research Center, Japan Atomic Energy Agency, 8-1 Umemi-dai, Kizu, Soraku, Kyoto 619-0215, Japan

Paolo Tomassini, Antonio Giulietti, and Danilo Giulietti
Intense Laser Irradiation Laboratory, IPCF, Area della Ricerca del CNR di Pisa via Moruzzi 1, 56124 Pisa, Italy
(Received 6 October 2005; published 16 March 2006)

We use a one-shot measurement technique to study effects of laser prepulses on the electron laser wakefield acceleration driven by relativistically intense laser pulses ($\lambda = 790$ nm, 11 TW, 37 fs) in dense helium gas jets. A quasimonoenergetic electron bunch with an energy peak ~ 11.5 MeV [$\Delta E/E \sim 10\%$ (FWHM)] and with a narrow-cone angle (0.04π mm mrad) of ejection is detected at a plasma density of 8×10^{19} cm^{-3}. A strong correlation between the generation of monoenergetic electrons and optical guiding of the pulse in a thin channel produced by picosecond laser prepulses is observed. This generation mechanism is well corroborated by two-dimensional particle-in-cell simulations.

DOI: 10.1103/PhysRevE.73.036407 PACS number(s): 52.38.Kd, 41.75.Jv, 52.38.Hb

I. INTRODUCTION

Among a number of concepts of the particle acceleration by laser fields, the laser wakefield acceleration (LWFA) in underdense plasma [1] provides one of the most promising approaches to high performance compact electron accelerators because it exploits ultrahigh gradients and high-frequency acceleration fields of the plasma wave. In principle, the LWFA with a few mm acceleration length driven by tens of TW laser pulses allows the generation of electron bunches with the kinetic energy of hundreds of MeV and with their duration of tens of fs. Until now, electron bunches with a maximal energy up to 200 MeV and a transverse emittance less than 0.1π mm mrad have been observed from helium gas jets irradiated by tens of TW laser pulses [2]. The duration of electron bunches are demonstrated to be less than 1 ps by the direct measurement of the coherent THz radiation from the jet plasma [3]. Recently, several measurements of the quasimonoenergetic electron acceleration by LWFA for very different plasma and laser parameters have been reported as well [4]. However, necessity of good reproducibility, high total charge, and lower energy spread of accelerated electrons requires seeking new approaches such as two-stage (injector and accelerator) schemes [5].

Usually an acceleration process consists of two distinct parts: electron injection and electron acceleration. Electron acceleration by the plasma wakefield has been a matter of study for many years [6] though processes of the injection of plasma electrons in the acceleration phase of the plasma field have yet to be well understood. The importance of injection is apparent; it results in the total charge, energy distribution, emittance, and bunch duration of accelerated electrons. The complexity of electron injection for monoenergetic LWFA is that it requires a very short duration of injected electron bunches. This cannot be achieved by applying conventional accelerators so that the development of injection schemes based on plasma processes called "self-injection" is necessary. Self-injection is especially important for two-stage LFWA schemes that are to utilize a high-density plasma injector and lower density capillary discharge [5] to provide a much lower energy spread of accelerated electrons.

For the acceleration driven by a single laser pulse, one of the simplest way to put energetic electrons into the acceleration phase of the wakefield is plasma-wave breaking [7,8]. This wave-breaking process is the randomization of regular oscillations of plasma electrons where the rate depends on plasma and laser pulse parameters [8,9]. The wave-breaking injection can be fast at steep density plasma interfaces that are very important for a tightly focused laser pulse. Due to the transverse wave breaking [10] only a few periods of

*Email address: hosokai@tokai.t.u-tokyo.ac.jp
†Also at A. M. Prokhorov General Physics Institute RAS, Vavilov street 38, Moscow 119991, Russia.

plasma waves remain intact behind such a laser pulse. Presently, a well collimated, ultrashort MeV electron bunch has been generated by the wave breaking using a shock wave driven by the irradiation of laser prepulses [11,12]. Such an electron bunch produced in the single-laser-pulse acceleration can be further accelerated in a lower density plasma; the so-called two-stage-acceleration scheme. The high-density injector provides a large total charge of accelerated electrons at their relatively small maximal energy while the accelerator (capillary discharge [5,13]) raises the energy of the electrons decreasing the energy spread considerably.

It has been also shown that the LWFA in dense gas jets is very sensitive to the laser prepulse parameters. Conditionally, a femtosecond laser pulse can be separated into three parts: the main femtosecond pulse, the nanosecond pedestal [amplified spontaneous emission (ASE)] with its intensity of $10^{-7}-10^{-6}$ of the main pulse, and the picosecond pedestal (optical leakage) with its intensity of $\sim 10^{-3}$ [14]. In higher density plasmas the nanosecond ASE pedestal forms a cavity with the shock wave at its edge that provokes the wave breaking of plasma waves [11,15]; results of higher intensity picosecond prepulses have yet to be studied. Though with lowering the plasma density effects of the prepulse can be reduced, the generation of electron bunches with higher total charge requires denser plasmas provoking stronger effects of the prepulse [16].

In this paper, we present results of single-shot measurements of parameters of plasmas produced by 11 TW, 37 fs laser pulse and accelerated electrons in dense He gas jets. The time-resolved single-short technique is used to study effects of the laser prepulse on the LWFA in the gas jet. A strong correlation between quasimonoenergetic distribution of accelerated electrons and an optical guiding of intense laser pulses through a channel produced by laser prepulses is discussed.

II. EXPERIMENTAL SETUP

The experiment is conducted at the nuclear engineering laboratory of the University of Tokyo. The experimental setup is shown in Fig. 1. A supersonic pulsed helium gas jet is settled in a vacuum chamber. This pulsed-slit gas jet is generated by a device consisting of a shock-wave-free slit nozzle and a solenoid fast pulse valve [17]. The nozzle that contours with minimum length is designed to be the form $M_e=5.0$ (the Mach number) flow for helium by a method of characteristics, which provides a technique for a properly designed contour of supersonic nozzle for shock-free, isentropic flow. The supersonic slit nozzle has a 1.2 mm width and 4.0 mm length at the rectangular exit as shown in the inset of Fig. 1. The pulse valve is driven for 1.8 ms per shot at a repetition rate of 0.1 Hz. The stagnation pressure of the valve can be varied up to 80 atm. With this pressure the density at the exit of the nozzle ranges up to 6×10^{19} cm^{-3}. The uniform density distributions with the sharp boundary of the slit gas jet near the exit are verified by interferometry.

The 17 TW Ti:sapphire laser system based on the chirped pulse amplification technique generates with the pulse energy up to 600 mJ, 37 fs laser pulses at a fundamental wavelength of 790 nm with a 10 Hz repetition rate. Presently, the laser power at the target in the vacuum chamber is up to 11 TW in the experiment. The repetition rate of the laser pulses on the target is reduced to a 0.1 Hz (1 shot per 10 s) to synchronize with the pulse-operated gas jet by a mechanical shutter set behind the exit of the regenerative amplifier (REGEN) of the laser system. A laser pulse with a diameter of 50 mm is delivered into the vacuum chamber and is focused to the position of ~ 100 μm from the front edge of the slit nozzle boundary at a height of 1.3 mm from the nozzle exit with an off-axis parabolic mirror (OAP) with a focal length of 178 mm $f/3.5$. The focal spot size is 8.0 μm in full width at $1/e^2$ of maximum with ~ 50 μm Rayleigh length. The maximum laser intensity on the target is estimated to be $I=2.2\times 10^{19}$ W/cm^2 so that the laser strength parameter a_0 exceeds 3.1. The contrast ratio of the main pulse to the (ASE) prepulse preceding it at 150 ps is typically 5×10^{-7} at fundamental wavelength, which is measured by a third order femtosecond cross correlator. For the nanosecond-scale prepulse, the pedestal can be controlled by the tuning of the Pockels cells inside the REGEN. According to our previous studies, the electron beam generation by the laser wakefields depends strongly on the prepulse condition [11,15].

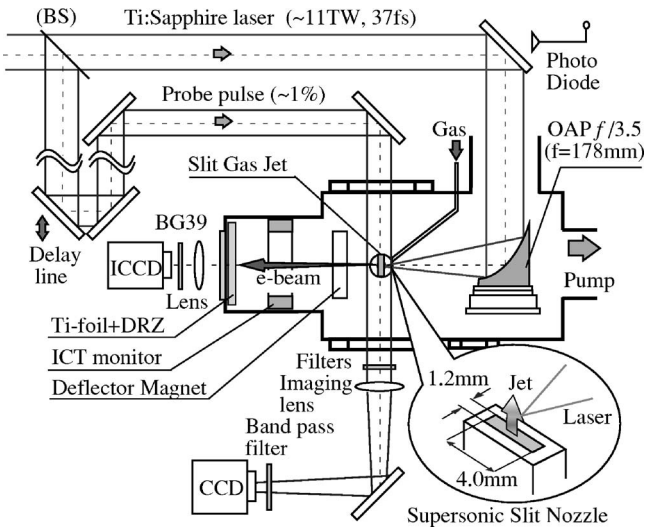

FIG. 1. Experimental setup. A supersonic slit nozzle is magnified in the inset.

In order to study the generation mechanism of a quasimonoenergetic electron beam from the plasma, the measurements of plasma density dynamics by the shadowgraph, the interferogram, the schlieren picture, the Thomson scattering of laser lights in the plasma, the spatial and energy distribution of the electron beam, and the charge are taken by one shot under the various prepulse condition. A part of the laser pulse carrying about 1% energy of the main pulse is divided through a 2 μm thickness Pellicle window (National Photocolor Co.) as a beam splitter (BS). It is delivered into the target region in the direction of 90° from the laser propagation axis and is used as a probe pulse for the plasma diagnosis. The shadowgraph image, the interferogram, and the schlieren picture of the plasma by this probe pulse, which provides a information on the density structure of the evolving plasma with a time resolution of $\leqslant$100 fs, is detected by

a 14 bit charge coupled device (CCD) camera. A band-pass filter ($\Delta\lambda=20$ nm at $\lambda=790$ nm) is put in front of the CCD to cut the plasma light. The polarization of the main laser pulse at the target can be chosen to be perpendicular or to be parallel to the probe beam axis using a pair of mirrors of the height shifter on the laser path. In the case of the main pulse with the parallel polarization, only the shadowgraph image of the plasma is detected. On the other hand, in the case of the main pulse with the perpendicular polarization, the image of the Thomson scattering lights from the plasma are overlapped in the shadowgraph image of the same plasma. The synchronization of the probe pulse with the evolving plasma is adjusted by the length of the optical path on the delay line. For taking interferograms or schlieren pictures a biprism or a wire target is installed behind the imaging lens, respectively.

The spatial distribution of the electron beam ejected from the gas jet is directly detected by a phosphor screen (KYOKKO Green X-ray intensifying screen DRZ) [18] put at the rear of the gas jet as shown in Fig. 1. The DRZ is sensitive to high-energy particles and radiations, which is set 110 mm away from the focus point behind a 300 μm titanium foil to avoid exposure to x rays, low-energy electrons, and the laser pulses. For measurements of the energy spectrum of the electron beam a magnetic electron deflector is set in the laser axis between the gas jet and the DRZ screen. The deflector consists of top and bottom arrays of magnets that act as a permanent dipole magnet to disperse the electrons according with their kinetic energy. In both cases, the scintillating images on the screen made by the deposited electrons are recorded by the image-intensified charge coupled device (ICCD) camera set behind the screen. In addition, a green-pass filter (Lambda Res.Opt. BG39) is put in front of the ICCD to reduce the background noise. This setup allows us to detect the energy spectrum of the electron beam from 6 to 40 MeV. The charge of the electron beam is measured by the integrated current transformer (ICT) set in the laser axis behind the gas jet. It has an entrance aperture of 40 mm with an acceptance cone angle of 25°.

III. EXPERIMENTAL RESULTS AND DISCUSSION

Four typical sequential shadowgraph images of the plasma from the time before the main pulse coming to the time after the main pulse passing are shown in Figs. 2(a)–2(d), respectively. The images are obtained for the gas density of 4.0×10^{19}cm^{-3} (plasma density of 8.0×10^{19} cm^{-3}) and the 11 TW peak power with 37 fs pulse duration of the main pulse with the smallest intensity of ASE accessible (prepulse with a contrast ratio of $\leqslant5\times10^{-7}$ at 150 ps and of $\leqslant1\times10^{-3}$ at 1 ps prior to the main pulse, pulse duration of these pedestal $\leqslant1$ ns with energy $\leqslant5\%$ of total pulse energy). For these conditions, a peaked spot distribution of high-energy electrons with an ejection cone angle $\leqslant2°$ is clearly observed on the center of the DRZ screen. The propagation direction of the laser pulses, focus point of the laser pulses and the gas jet area are marked in Fig. 2 by arrows and lines. The polarization of the main laser pulse is parallel to the probe beam axis.

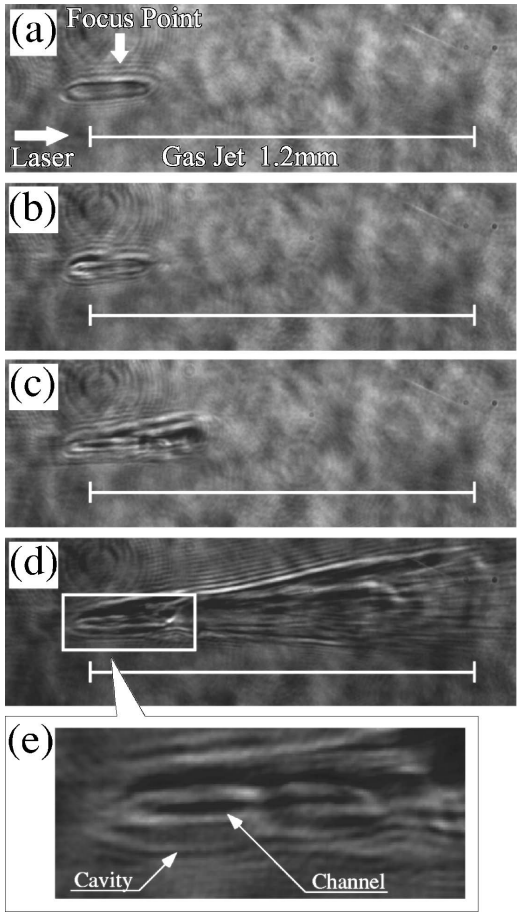

FIG. 2. Typical sequential shadowgraph images of the plasma for a gas density of 4×10^{19} cm^{-3} (plasma density of 8×10^{19} cm^{-3}) and a laser power of 11 TW. (a) 1.5 ps before the main pulse, (b) the time where just the main pulse comes to the focus point, (c) 1.2 ps after t he main pulse, (d) 5.2 ps after the main pulse, and (e) the magnified image of the cavity region in (d).

In Fig. 2(a), a long elliptical preplasma cavity expanding from the focus point (~100 μm from the front edge of the nozzle) is shown at 1.5 ps before the main pulse comes to the focus point. It has a size of $\sim50\times\sim300$ μm in the transverse and the laser propagation direction. It is known that in the case of short Rayleigh length, the ns-scale prepulse can form a cavity and modify the density structure generating a shock wave in front of the laser propagation [11,15]. The outershell of the cavity by the shock wave is seen in Fig. 2(a). Also a faint channel-like structure on the center axis inside the cavity exhibited there as well. After that, the channel-like structure inside the cavity rapidly grows, which is clearly displayed in Fig. 2(b) at the moment just before the main pulse coming to the focus point. We attribute the appearance of channel-like structure in the cavity to the focusing of the high-intensity picosecond scale prepulse. A few ps before the main pulse the focusing intensity of the ps-pedestal exceed 10^{16} W/cm^2. The ps prepulse in some shots can be extra-focused due to its refraction in the plasma cavity forming a channel with ponderomotively evacuated electrons outside it. At 1.2 ps after the main pulse has passed the focus

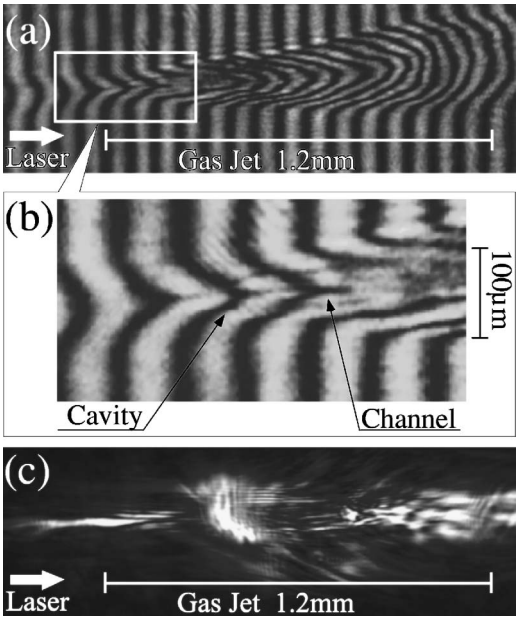

FIG. 3. Typical interferograms and schlieren pictures of the plasma for a density of 4×10^{19} cm^{-3} (plasma density of 8×10^{19} cm^{-3}) and a laser power of 11 TW. (a) at 5.2 ps after the main pulse corresponding to 2(d), (b) a magnified image of the cavity region in (a), and (c) typical schlieren pictures of the plasma corresponding to 2(d).

point, [see Fig. 2(c)], a part of the main pulse, can be refracted along the cavity by its density effects [15] and the channel-like structure inside the cavity becomes distinct. At 5.2 ps after the main pulse has past [see Fig. 2(d)], a lot of channels expand to the rear of the cavity. Figure 2(e) shows a magnified picture of the cavity region indicated by a rectangle in Fig. 2(d). Though this image is affected by the laser postpulses, the cavity and the narrow channel-like structure inside the cavity can be still clearly seen.

To confirm the narrow channel formation inside the cavity, we measure the density profile of the plasma with interferograms and schlieren pictures under the same gas density; the peak power of main pulse and prepulse conditions as given in Fig. 2. Figure 3(a) shows a typical interferogram of the plasma at $t=5.2$ ps. A magnified picture of the cavity region indicated by a rectangle in Fig. 3(a) is given in Fig. 3(b). Figure 3(c) shows a typical schlieren picture of the plasma at the same time $t=5.2$ ps. According to the interferograms, the laser pulse modifies the density distribution of the gas jet along its paths. The shifted fringes around the focus position in Fig. 3(a) corroborate well by the cavity formation. In addition, the formation of a narrow density channel with width of $\leqslant 10$ μm on the axis inside the cavity is seen in Fig. 3(b), which is consistent with the channel-like structure formation as in Fig. 2. According to the schlieren picture, one can see a narrow straight channel at the cavity region which coincides with the one in Figs. 2 and 3(b) as well. They corroborate well the narrow density channel formation inside the cavity.

In order to find a correlation between the channel formation and the electron acceleration by laser wakefields we perform electron energy distribution measurements with the

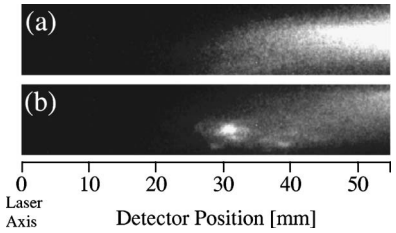

FIG. 4. Typical images of electron deposition on the DRZ screen behind the magnetic defrector for a gas density of 4×10^{19} cm^{-3} (plasma density of 8×10^{19} cm^{-3}) and of 11 TW laser pulse. (a) a 100% energy spread spectrum case; (b) a quasimonoenergetic spectrum case.

setup described in the previous section. Figures 4(a) and 4(b) show the typical images of the deposition of electrons on the DRZ screen behind the magnetic deflector. The energy spectra of electrons shown in (a) and (b) in Fig. 5 are converted from the image of Figs. 4(a) and 4(b) respectively. Both electron beams of high energy over 6 MeV with a narrow cone angle $\leqslant 4°$ and with quasimonoenergetic spectrum can be produced under the smallest ASE prepulse condition mentioned above and the gas density of $\sim 4\times10^{19}$ cm^3 (plasma density of 8.0×10^{19} cm^{-3}). Under these conditions, the energy spectrum of the accelerated electrons in the plasma usually exhibits the 100% spread distribution but it exhibits the quasimonoenergetic distribution frequently. We notice here that the electron energy spectrum has a specific form with the cut at the maximal energy and a pedestal at the lower energy

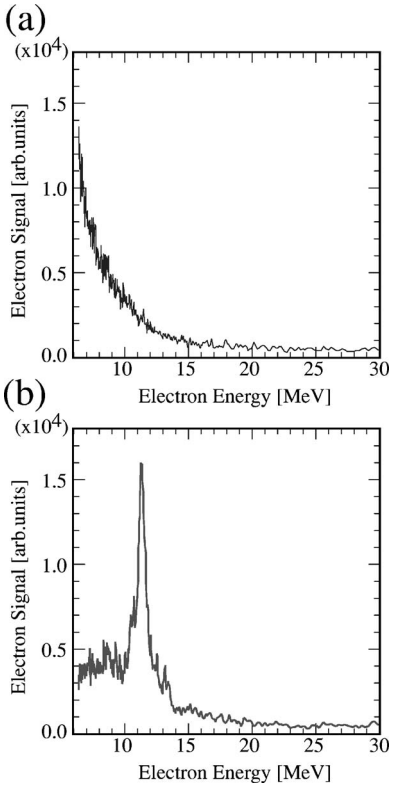

FIG. 5. Typical energy spectra of accelerated electrons converted from the images of Fig. 4. (a) a 100% energy spread spectrum case; (b) a quasimonoenergetic spectrum case.

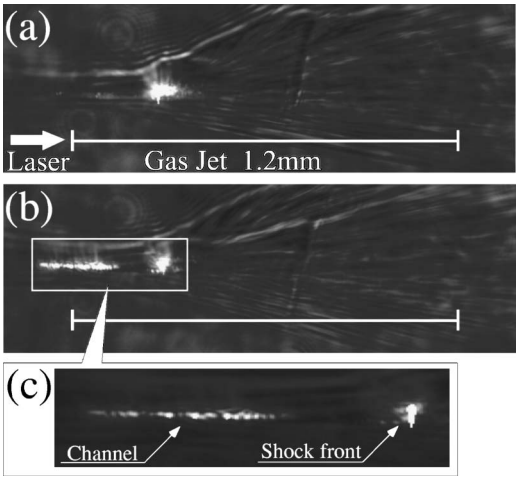

FIG. 6. Typical shadowgraph images of the plasma overlapped with Thomson scattering of the laser light in the plasma at 5.2 ps after the main pulse for gas density $N=4\times10^{19}$ cm^{-3} (plasma density $N_e=8\times10^{19}$ cm^{-3}) and a laser power of 11 TW. (a) a 100% energy spread spectrum case; (b) a quasimonoenergetic spectrum case; (c) a magnified image of the cavity region in (b).

side as it has been described theoretically in Ref. [19]. The peak value of ~11.5 MeV on the spectrum is reproducible as long as it appears under this condition. The peak distribution (b) in Fig. 5 exhibits the smallest energy spread of $\Delta E/E\sim10\%$ in full width at half maximum (FWHM) in our recent experiment; it practically fluctuates within the range of $\Delta E/E<35\%$ (FWHM) time by time. According to Fig. 4(b), the size of the spot of the quasimonoenergetic electrons of ~11.5 MeV is 2.0 mm (FWHM), which corresponds to a divergence angle of the ejection of 1.0°. The corresponding transverse geometrical emittance of the quasimonoenergetic electrons is as small as 0.04π mm mrad.

To reveal the source of the generation of monoenergetic electrons, we measure the Thomson scattering of the laser light with the shadowgraph. For that we change the polarization plane of the laser pulse from perpendicular to the probe pulse axis. By choosing this polarization of the laser pulse the Thomson scattering of laser light emits in the same direction of the probe pulse propagation. Figures 6(a) and 6(b) show two typical cases of Thomson scattering of the laser light from the plasma overlapped with the shadowgraph image at 5.2 ps after the main pulse has passed. They are obtained under the same gas density, peak power of the main pulse and prepulse conditions as given in Fig. 2. These images are obtained coincidently with the corresponding energy spectra of electrons by one shot. The temporal resolution of the shadowgraph images depends on the duration of the probe pulse ($\leqslant$100 fs), while the Thomson scattering lights in the same image have only ~1 ps temporal resolution. Because the Thomson scattering light is generated by the main pulse propagating through the plasma, the maximum duration of the emission depends on the plasma length. The images of Figs. 6(a) and 6(b) correspond to the 100% energy spread spectrum of Fig. 5(a) or the monoenergetic spectra of Fig. 5(b), respectively. In case the electrons exhibit 100% energy spread distribution as shown in Fig. 6(a), a bright

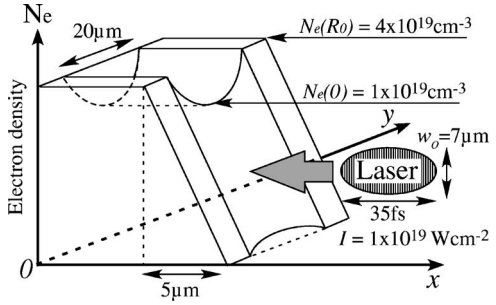

FIG. 7. Plasma and laser parameters for a 2D-PIC simulation.

Thomson scattering light emission is observed only at the rear side of the cavity edge. In case the electrons exhibit the quasi monoenergetic distribution as shown in Fig. 6(b), in contrast, the bright Thomson scattering light emissions are observed not only at the rear side of the cavity edge but inside the cavity with a line shape over 300 μm along the center axis. Figure 6(c) shows the magnified image of the cavity region indicated by a rectangle in Fig. 6(b) to definite the emitting points in this straight channel. As shown in Fig. 6(c) the line-shaped Thomson scattering light consists of many bright dots periodically lying on the center axis. Generally, the strong wave breaking can be expected at the positions where the Thomson light emits brightly because the intensity of the Thomson scattering light is dominated by the plasma density and the laser intensity. This is the apparent evidence of laser propagation with hopping (periodically focusing and defocusing) by the optical guiding in the narrow channel. The guiding length of this channel is over 300 μm which is corresponding to over 6 times the Rayleigh length.

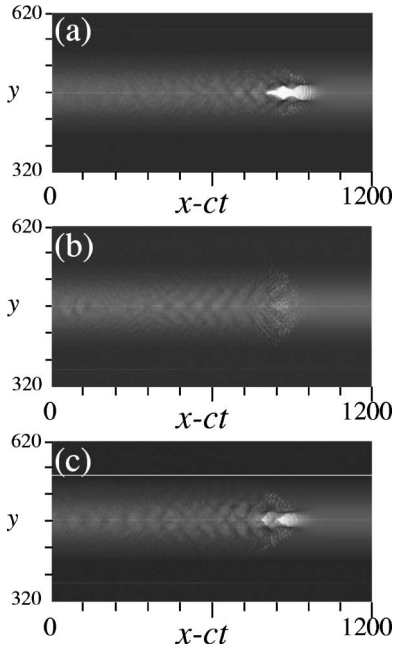

FIG. 8. Spatial distributions of the normalized electron density at (a) 0.59 ps, (b) 0.98 ps, and (c) 1.37 ps, respectively, after the laser injection into the plasma channel. Laser intensity is $I=1\times10^{19}$ W cm^{-2}.

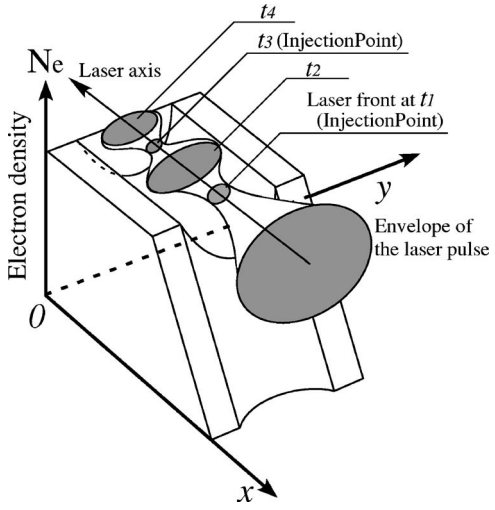

FIG. 9. Illustration of the laser propagation in the channel obtained by the 2D-PIC simulation.

As the pedestal of the laser pulse increases longer, the plasma cavity expands larger and the emission point of the Thomson scattering light at the cavity edge shifts to the rear side with the shock front. It is beyond doubt that the bright Thomson scattering light at the cavity edge shown in Fig. 6 corroborates the steep high-density ramp at the cavity edge produced by the expanding shock front. On the other hand, as the pedestal of the laser pulse increases longer, the bright dots of the Thomson scattering light lying on the axis in the cavity as shown in Figs. 6(b) and 6(c) disappear, and the energy distribution of the electrons changes to the 100% one as well. It means that the generation of the quasimonoenergetic electrons depends strongly on the channel formation process in the cavity so that the laser focus position and prepulse condition become crucial parameters for it. In this case, the effective focus point for the main pulse shifts ~ 200 μm to the upstream from the initial focusing point due to the channel formation in the cavity by ns and ps laser prepulses.

The charge of the accelerated electrons obtained by the ICT is approximately 10 pC, which is no significant change between the 100% energy spread case and the quasimonoenergetic case because it seems to be dominated by low-energy electrons below few MeV. However the total charge can be underestimated by ICT measurement.

IV. PARTICLE IN CELL SIMULATION

To understand the hot-spotted Thomson scattering of the laser pulse seen in the pre-pulse-produced channel we perform fully relativistic 2D particle in cell (PIC) simulations (see also Ref. [20]) with code FPLaser2D [21]. The FPLaser2D code employs the "moving window" technique. The size of the window moving at the speed of light in vacuum is 164 μm$\times$120 μm (2800$\times$2048 cells) and we used 16 particles per cell. No plasma ionization is included.

Plasma and laser parameters are shown in Fig. 7: the plasma channel with radius of $R_0=10$ μm is irradiated by an *s*-polarized laser pulse with an initial waist size of $w_0=7$ μm, duration of $\tau=35$ fs, and its intensity of $I=1\times10^{19}$ W cm^{-2} ($a_0=2$). In both cases the laser intensity to exceed the critical power for self-focusing $P_{cr}=17.4(N_{cr}/N_e)$ (GW), here N_e is the electron density and N_{cr} is the critical density for the laser light. The minimal electron density in the channel is $N_e(0)=1\times10^{19}$ cm^{-3} and the maximal $N_e(R_0)=4\times10^{19}$ cm^{-3}. The electron density length at a vacuum-plasma interface is set to 5 μm.

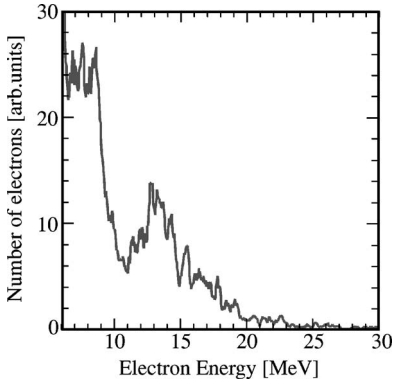

FIG. 10. The energy spectrum of the accelerated electrons from the 2D-PIC simulation.

Dynamics of the spatial distribution of an electron density in the plasma interacting with the laser pulse $I=1\times10^{19}$ W cm^{-2} is shown in Fig. 8. Periodical focusing and defocusing of the pulse in the channel can be seen in Fig. 8. (This process is illustrated by Fig. 9.) Strong wave breaking appears in the vicinity of strong self-focusing procuring electron injection. As seen in Fig. 8 the length of the injection is the order of a plasma wavelength that provides very short duration of injected bunch. As a result, one can see the peak distribution of accelerated electrons at energy $\epsilon=12$ MeV as shown in Fig. 10. (Here, we should note that there is no spatial resolution between high- and low-energy electrons in the PIC simulation.) However, the focusing length ~ 100 μm exceeds that of which were measured in the channel. To understand dynamics of waist radius, w, we use a form of a paraxial equation derived in Refs. [22,23]. In a plasma channel with parabolic density distribution $N_e(r)=N_e(0)+N_e(R_0)r^2/R_0^2$, where R_0 is the channel radius and r is the transverse coordinate; it can be presented in the following form:

$$\frac{d^2R}{dx^2}=\frac{2}{kL_R}\frac{1}{R^3}-\frac{N_e(0)}{N_{cr}}\left(\frac{w_0}{R_0}\right)^2\frac{R}{\gamma}-\frac{N_e(0)}{N_{cr}}\frac{a_0^2}{4\gamma R^3}-\frac{4}{kL_R}\frac{a_0^2}{\gamma^2}\left[\frac{1}{R^5}-\left(\frac{w_0}{R_0}\right)^2\frac{1}{R^3}\right]+\frac{2}{kL_R}\frac{a_0^4}{\gamma^4R^7},$$

where w_0 is the initial waist size, $L_R=kw_0^2$ is the Rayleigh length, a_0 the normalized laser field, $R=w(x)/w_0$, x is the direction of laser pulse propagation normalized on w_0, $k=w/c$, and $\gamma=(1+a_0^2/2)^{1/2}$. For a weak relativistic case $a_0\sim1$, the minimal radius can be estimated at $R''=0$ that gives $w_{min}=w_0(\omega R_0/2\omega_{pl}L_R)^{1/2}$; here ω and ω_{pl} are laser and plasma frequencies, respectively. This means that a laser pulse with a moderate intensity can be strongly focused if

$\omega R_0/2\omega_{pl}L_R \ll 1$. This strong focusing is also accompanied by electron depletion with forming both steep transverse and steep longitudinal density gradients. After that the pulse has to diffract. The typical self-focusing length equals $X=\omega R_0/\omega_{pl}$. Because the diffraction term at high a_0 is proportional to R^{-7} the length of vicinity $w \sim w_{min}$ is about few w_0. If $\Delta X \approx \lambda_{pl}=2\pi c/\omega pl$ we may expect a strong longitudinal wave breaking with an injection of low-emittance electrons in the accelerating phase of the plasma wake; here, λ_{pl} is a plasma wavelength. Moreover, if the acceleration length is equal to the detuning length [22] $L_D=2\pi c\omega^2/\omega_{pl}^3$ or $R_0=\lambda N_{cr}/N_e$ the beam of accelerated electrons can be monoenergetic; here, λ is a laser wavelength. Some discrepancies in calculated and measured distributions of hot spots in the plasma channel may be caused by the numerical difference in R_0 and ω_{pl}.

V. CONCLUSION

We have applied a one-shot measurement technique to study the effects of laser prepulses on the electron laser wakefield acceleration driven by a relativistically intense laser pulses. Time-resolved shadowgraph images, Thomson scattering, and schlieren pictures in *s*- and *p*-polarized planes have clearly shown the formation of the plasma cavity with a shock wave in its front. Time-resolved interferograms and shadowgraph images have proved the appearance of a narrow plasma channel several picoseconds before main pulse coming. The hot-spotted distribution of the scattered laser light has been observed in the channel. We attributed this effect to regular focusing and defocusing (hopping) of the laser pulse in the channel. According to the numerical simulation this hopping is accompanied by the rapid self-injection of plasma electrons in the accelerating phase of a laser wake that gives a quasimonoenergetic distribution of accelerated electrons. The strong correlation between the generation of monoenergetic electrons and optical guiding of the pulse in a thin channel produced by picosecond laser prepulses has been observed. In the absence of the channel the electron distribution is a Maxwell-like. A quasimonoenergetic electron bunch with an energy peak $\sim$11.5 MeV [$\Delta E/E \sim 10\%$ (FWHM)], with a transverse geometrical emittance of 0.04π mm mrad and with the total charge over 10 pC has been detected at a plasma density of 8×10^{19} cm^{-3}.

ACKNOWLEDGMENTS

This research was partly supported by the advanced compact accelerator Development Office of the NIRS (National Institute of Radiological Sciences) Japan.

[1] T. Tajima and J. M. Dawson, Phys. Rev. Lett. **43**, 267 (1979).
[2] J. Faure, V. Malka, and J.-R. Marques, Phys. Plasmas **7**, 3009 (2000); V. Malka, S. Fritzler, and E. Lefebvre, Science **298**, 1596 (2002); C. B. Schroeder, E. Esarey, and C. G. R. Geddes, Phys. Plasmas **10**, 2039 (2003).
[3] W. P. Leemans, C. G. R. Geddes, and J. Faure, Phys. Rev. Lett. **91**, 074802 (2003); P. Catravas, E. Esarey, and W. P. Leemans, Phys. Plasmas **9**, 2428 (2002); W. P. Leemans, J. van Tilborg, and J. Faure, *ibid.* **11**, 2899 (2004).
[4] S. P. D. Mangles, C. D. Murphy, and Z. Najmudin, Nature (London) **431**, 535 (2004); C. G. R. Gedds, Cs. Toth, and J. van Tilborg, *ibid.* **431**, 538 (2004); J. Faure, Y. Glinec, and A. Pukhov, *ibid.* **431**, 541 (2004); E. Miura, K. Koyama, and S. Kato, Appl. Phys. Lett. **86**, 251501 (2005); A. Yamazaki, H. Kotaki, and I. Daito, Phys. Plasmas **12**, 093101 (2005).
[5] T. Hosokai, M. Kando, H. Dewa, H. Kotaki, S. Kondo, N. Hasegawa, K. Horioka, and K. Nakajima, Opt. Lett. **25**, 10 (2000).
[6] A. Modena, Z. Najmudin, and A. E. Dangor, Nature (London) **377**, 606 (1995); K. Nakajima, D. Fisher, and T. Kawakubo, Phys. Rev. Lett. **74**, 4428 (1995); F. Amiranoff, S. Baton, and D. Bernard, *ibid.* **81**, 995 (1998); F. Dorchies, F. Amiranoff, and V. Malka, Phys. Plasmas **6**, 2903 (1999).
[7] S. V. Bulanov, V. I. Kirsanov, and A. S. Sakharov, JETP Lett. **53**, 565 (1991); R. G. Hemker, K.-C. Tzeng, W. B. Mori, C. E. Clayton, and T. Katsouleas, Phys. Rev. E **57**, 5920 (1998); T. V. Liseikina, F. Califano, V. A. Vshivkov, F. Pegoraro, and S. V. Bulanov, *ibid.* **60**, 5991 (1999); R. G. Hemker, N. M. Hafz, and M. Uesaka, Phys. Rev. ST Accel. Beams **5**, 041301 (2002); A. Pukhov and J. Meyer-Ter-Vehn, Appl. Phys. B: Lasers Opt. **74**, 355 (2002).
[8] S. Bulanov, N. Naumova, F. Pegoraro, and J. Sakai, Phys. Rev. E **58**, R5257 (1998); H. Suk, N. Barov, J. B. Rosenzweig, and E. Esarey, Phys. Rev. Lett. **86**, 1011 (2001); P. Tomassini, M. Galimberti, and A. Giulietti, Laser Part. Beams **22**, 423 (2004); P. Tomassini, M. Galimberti, and A. Giulietti, Phys. Rev. ST Accel. Beams **6**, 121301 (2003).
[9] T. Ohkubo, A. Zhidkov, T. Hosokai, K. Kinoshita, and M. Uesaka Phys. Plasmas (to be published).
[10] S. V. Bulanov, F. Pegoraro, A. M. Pukhov, and A. S. Sakharov, Phys. Rev. Lett. **78**, 4205 (1997); S. V. Bulanov, F. Califano, and G. I. Dudnikova, Plasma Phys. Rep. **25**, 468 (1999).
[11] T. Hosokai, K. Kinoshita, A. Zhidkov, K. Nakamura, T. Watanabe, T. Ueda, H. Kotaki, M. Kando, K. Nakajima, and M. Uesaka, Phys. Rev. E **67**, 036407 (2003).
[12] D. Giulietti and M. Galimberti, Phys. Plasmas **9**, 3655 (2002).
[13] N. E. Andreev, S. V. Kuznetsov, and I. V. Pogorelsky, Phys. Rev. ST Accel. Beams **3**, 021301 (2000).
[14] K. Kinoshita, T. Hosokai, A. Zhidkov, T. Ohkubo, N. Yamaoka, A. Maekawa, and M. Uesaka Jpn. J. Appl. Phys. (to be published); P. McKenna, K. W. D. Ledingham, and I. Spencer, Central Laser Facility, CLRC Rutherford Appleton Laboratory Annual Report 2001/2002, 79 2002, (unpublished).
[15] T. Hosokai, K. Kinoshita, A. Zhidkov, K. Nakamura, H. Kotaki, M. Kando, K. Nakajima, and M. Uesaka, Phys. Plasmas **11**, L57 (2004).
[16] M. Kando, S. Masuda, A. Zhidkov, A. Yamazaki, H. Kotaki, S. Kondo, T. Homma, S. Kanazawa, K. Nakajima, Y. Hayashi, M. Mori, H. Kiriyama, Y. Akanane, N. Inoue, H. Ueda, Y. Nakai, K. Tsuji, Y. Yamamoto, K. Yamakawa, J. Koga, T. Hosokai, M.

Uesaka, and T. Tajima, Phys. Rev. E **71**, 015403(R) (2005).
[17] T. Hosokai, K. Kinoshita, T. Watanabe, K. Yoshii, T. Ueda, A. Zhidkov, and M. Uesaka, *Proceedings of 8th European Particle Accelerator Conference* (EPS-IGA and CERN, Paris, 2002), p. 1989; J. D. Anderson, Jr., *Modern Compressible Flow with Historical Perspective*, 2nd ed. (Mc Graw Hill, New York, 1989), Chap. 5.
[18] http://www.kasei-optonix.co.jp/english/products/x-ray/kyokko.html
[19] S. V. Bulanov and T. Tajima, J. Part. Accel. Soc. Jpn. **2**, 35 (2005); S. V. Bulanov, M. Yamagiwa, and T. Zh. Esirkepov, Phys. Plasmas **12**, 073103 (2005); A. Yamazaki, H. Kotaki, and I. Daito, *ibid.* **12**, 093101 (2005).
[20] T. Ohkubo, S. V. Bulanov, and A. Zhidkov (unpublished).
[21] A. Zhidkov, J. Koga, T. Hosokai, K. Kinoshita, and M. Uesaka, Phys. Plasmas **11**, 5379 (2004).
[22] E. Esarey, P. Sprangle, J. Krall, and A. Ting, IEEE Trans. Plasma Sci. **24**, 252 (1996).
[23] H. S. Brandi, C. Manus, G. Mainfray, and T. Lehner, Phys. Rev. E **47**, 3780 (1993); H. S. Brandi, C. Manus, G. Mainfray, T. Lehner, and G. Bonnaud, Phys. Fluids B **5**, 3539 (1993).